

**Tolerance for Li dendrite penetration in Ta-doped  $\text{Li}_7\text{La}_3\text{Zr}_2\text{O}_{12}$  solid electrolytes sintered with  $\text{Li}_{2.3}\text{C}_{0.7}\text{B}_{0.3}\text{O}_3$  additive**

Hiromasa Hosokawa, Atsuto Takeda, Ryoji Inada\*, Yoji Sakurai

Department of Electrical and Electronic Information Engineering, Toyohashi University of Technology,  
1-1 Hibarigaoka, Tempaku-cho, Toyohashi, Aichi 441-8580, Japan.

\*Corresponding author:

Phone: +81-532-44-6723, Fax: +81-532-44-6757, E-mail address: inada.ryoji.qr@tut.jp

**Abstract**

We fabricated garnet-type Ta-doped  $\text{Li}_7\text{La}_3\text{Zr}_2\text{O}_{12}$  (LLZTO) /  $\text{Li}_{2.3}\text{C}_{0.7}\text{B}_{0.3}\text{O}_3$  (LCBO) composite ceramic solid electrolytes. By adding the appropriate amount of LCBO to LLZTO, composite solid electrolytes were densified by sintering at 1000°C without covering the pellet with LLZTO mother powder. LLZTO/LCBO Composites with LCBO volume contents of 20 and 50% showed the ionic conductivity well above  $1 \times 10^{-4} \text{ S cm}^{-1}$  at room temperature. Li plating and stripping property for LLZTO/LCBO composites was evaluated using symmetric cells with Li metal electrodes at room temperature. As results, a symmetric cell composed of composite solid electrolyte with low LCBO volume content was stably cycled at the current density up to  $0.3 \text{ mA cm}^{-2}$ , but increasing the amount of LCBO significantly lowered the current density where the Li dendrite penetration in solid electrolyte occurs. This indicates that LCBO addition is effective for lowering the sintering temperature of LLZTO but the smaller LCBO content is prefer to maintain the tolerance for Li dendrite penetration at high current density.

**Keywords:** solid electrolyte, garnet, composite, ionic conductivity, Li dendrite

**1. Introduction**

All-solid-state Li-based batteries are expected as one of the next generation energy stored devices because of their high energy density, high safety and excellent cycle stability [1]. Development of inorganic solid Li-ion conducting materials for the use as solid electrolyte is most important issue to realize all-solid-state batteries. The materials used for solid electrolyte must have not only high Li-ion conductivity above  $10^{-3} \text{ S cm}^{-1}$  at room temperature but also chemical stabilities against both cathode and anode materials, air

and moisture. Although oxide based solid electrolyte materials have rather lower conductivity than sulfide based one, they have other advantages such as their chemical stability and handling [1, 2].

Among the various kinds of oxide solid electrolytes, Li-stuffed garnet-type oxide with the formula of  $\text{Li}_7\text{La}_3\text{Zr}_2\text{O}_{12}$  (LLZO) have attracted much attention for the application to solid-state batteries, because of their high ionic conductivity of  $10^{-4}$ – $10^{-3}$  S  $\text{cm}^{-1}$  at room temperature, excellent thermal performance and stability against Li metal anode with the lowest electrode potential and high gravimetric theoretical capacity (= 3860 mAh  $\text{g}^{-1}$ ) [3, 4]. In general, high temperature sintering at 1100–1200°C is required for the densification of LLZO. In order to suppress significant Li loss from LLZO during the sintering process and secondary phase formation, LLZO pellet must be covered by the LLZO mother powder [3, 4]. Since this mother powder cannot be reused, this process leads to lowering the material yield and increasing the production costs of LLZO. To address this issue, adding  $\text{Li}_3\text{BO}_3$  (LBO) with low melting point has been proposed for sintering LLZO at low temperature [5–8]. By adding proper amount of LBO on LLZO, dense composite solid electrolytes with room temperature conductivity above  $1 \times 10^{-4}$  S  $\text{cm}^{-1}$  have been successfully fabricated at the sintering temperature from 800 to 1000°C without using mother powder. Lowering the sintering temperature results into not only the reduction of processing cost of LLZO but also the fabrication of solid-state batteries via co-sintering process with electrode active materials without causing undesired side reaction [7, 9]. In these previous works, however, little has been investigated about the stability at the interface between the composite solid electrolyte and high capacity Li metal electrode during the charge (Li plating) and discharge (Li stripping) cycling.

In this work, we fabricated composite ceramic solid electrolytes with garnet-type Ta-doped LLZO ( $\text{Li}_{6.55}\text{La}_3\text{Zr}_{1.55}\text{Ta}_{0.45}\text{O}_{12}$ , LLZTO) and  $\text{Li}_{2.3}\text{C}_{0.7}\text{B}_{0.3}\text{O}_3$  (LCBO). Since LCBO has a melting temperature as low as 700°C and moderate ionic conductivity of  $10^{-7}$ – $10^{-6}$  S  $\text{cm}^{-1}$  at room temperature [10–12], it is expected that LCBO works as a sintering aid for LLZTO at lower temperature. In addition, LCBO shows excellent electrochemical stability against Li metal [13]. The effect of LCBO additive on crystal phase, microstructure and ionic conductivity of LLZTO/LCBO composites were evaluated and electrochemical Li plating and stripping performance of LLZTO/LCBO composites was investigated.

## 2. Experimental

Both LLZTO and LCBO powders were prepared via a simple solid state reaction method and the

details are described in the supplementary information. Obtained LLZTO and LCBO powders were mixed in an agate mortar with the LCBO contents of 20 and 50% in volume (corresponding to the LCBO contents of 8.9% and 28% in weight). The mixed powders were pelletized by cold isostatic pressing at 300 MPa and then sintered at 1000°C for 15 h in air using Pt-Au5% alloy crucible. At the sintering process, the composite pellets were not covered with the LLZTO mother powder, which is commonly used to suppress the loss of Li during high temperature sintering process and the formation of secondary phases [3, 14–16]. For comparison, LLZTO pellet sample without LCBO additive was also prepared by sintering at 1150 °C for 15 h with mother powder using Pt-Au5% alloy crucible. The crystal phase of the composite pellet was evaluated by X-ray diffraction (XRD, RIGAKU Multiflex) using  $\text{CuK}\alpha$  radiation ( $\lambda = 0.15418$  nm). Fractured surface microstructure of each sintered pellet was observed by field-emission scanning electron microscope (FE-SEM, Hitachi High-Technologies SU8000 Type II).

To evaluate the stability of interface between LLZTO/LCBO composite solid electrolyte and Li metal, we constructed symmetric cells in Ar-filled glove box, by attaching Li metal foils (diameter = 8 mm and thickness = 0.15 mm) on top and bottom end surfaces of composite solid electrolyte (thickness = 1.60 mm). Before attaching Li foils, both the top and bottom surfaces were mechanically polished and coated by Au thin films (thickness = 150 nm). Then, heat treatment at 175°C and 5 hours was applied to a symmetric cell after cell construction to reduce the interfacial charge-transfer resistance  $R_{\text{int}}$  between solid electrolyte and Li metal [15–20].  $R_{\text{int}}$  and ionic conductivity of LLZTO and LLZTO/LCBO composites were evaluated at 27°C by measuring electrochemical impedance of symmetric cell using an impedance meter (HIOKI IM3536). Li plating and stripping properties was also investigated at 25°C by a galvanostatic cycling test of each symmetric cell using Battery Test System (TOSCAT-3100, Toyo System).

### 3. Results and discussion

Fig. 1(a) shows XRD patterns for As-synthesized LCBO and LLZTO powders. The calculated patterns for  $\text{Li}_2\text{CO}_3$  and cubic LLZO garnet using their structural data are also plotted as the references [10, 21]. As synthesized LCBO powder has a  $\text{Li}_2\text{CO}_3$ -like structure but the diffraction peaks at  $2\theta = 29\text{--}35^\circ$  and  $47\text{--}50^\circ$  are shifted remarkably towards lower angle, which is mainly attributed to the increase in a lattice size along a  $c$ -axis by substituting  $\text{C}^{4+}$  with  $\text{B}^{3+}$  with larger ionic radius [10–12]. On the other hand, as-synthesized LLZTO powder has a cubic garnet structure but the diffraction peaks are shifted slightly towards higher

angle, due to the decrease in a lattice size by substituting  $Zr^{4+}$  with  $Ta^{5+}$  with smaller ionic radius [14, 15]. The XRD patterns for sintered LLZTO and LLZTO/LCBO composites are summarized in Fig. 1(b). As well as sintered LLZTO without LCBO additive, the main phase of sintered LLZTO/LCBO composites is confirmed to be cubic garnet phase and almost no peaks from LCBO phase was observed, indicating that LCBO exists as amorphous phase in LLZTO/LCBO composites. Similar results are confirmed in sintered LLZO with LBO additive [5–8]. The lattice parameters and chemical compositions for all sintered samples are summarized in Table S1 and S2 in supplementary information.

Fig. 2 shows the comparison of fractured cross-sectional surfaces for sintered LLZTO and LLZTO/LCBO composites observed by FE-SEM. As shown in Fig. 2(a), average grain size in the sintered LLZTO without LCBO additive is 5–10  $\mu\text{m}$  and all grains are in good contact with each other to form a dense structure. Relative density of LLZTO pellet sintered at 1150°C was confirmed to be 93%. On the other hand, LLZTO/LCBO composites have quite different microstructure. The composites has a structure in which a paste-like substance is embedded between LLZTO grains with the size of approximately 5  $\mu\text{m}$ . This paste-like substance is considered to be amorphized LCBO and more uniformly distributed in the composite with a larger LCBO content. We roughly estimated the relative densities of LLZTO/LCBO composites taking into account the density of each pellet (calculated by the weight and geometrical parameters of each pellet), the content of LLZTO and LCBO at mixing stage and true densities of LLZTO ( $= 5.368 \text{ g cm}^{-3}$ ) and LCBO ( $= 2.096 \text{ g cm}^{-3}$ ). As results, the relative densities for LLZTO/LCBO composites with LCBO contents of 20% and 50% were confirmed to be 88% and 91%, respectively.

Fig. 3 shows the Nyquist plots of electrochemical impedance measured at 27°C for symmetric cells composed of LLZTO and LLZTO/LCBO composite pellets and Li metal electrodes. For all symmetric cells, the plot has two semicircles before applying heat treatment. After heating each cells at 175 °C for 5 hours, the diameter of semicircle at lower frequency range is significantly reduced while the semicircle at higher frequency range does not change significantly. By addressing this fact, the distorted semicircle at higher frequency range in each symmetric cell corresponds to the resistance for Li-ion conduction in each sintered pellet while the semicircle at lower frequency range reflects to the interfacial charge transfer resistance  $R_{\text{int}}$  between Li metal and solid electrolyte. Disappearing the semicircle at lower frequency range after the heat treatment is attributed to the reduction in  $R_{\text{int}}$ , due to the improvement of connectivity between Li metal and solid electrolyte [4, 15, 17–20]. In Fig. 3(a), area specific resistance (ASR) of sintered LLZTO is estimated

to be approximately  $170 \Omega \text{ cm}^2$  and  $R_{\text{int}}$  is approximately  $15 \Omega \text{ cm}^2$ . Using the thickness of the pellet ( $= 0.16 \text{ cm}$ ), the total (grain + grain-boundary) ionic conductivity at  $27^\circ\text{C}$  for LLZTO is calculated to be  $9.4 \times 10^{-4} \text{ S cm}^{-1}$ , agree well with the data in our previous works [14–16]. For comparison, ASR of LLZTO/LCBO composites is confirmed to be  $600\text{--}700 \Omega \text{ cm}^2$  and much larger than sintered LLZTO without LCBO additive (Fig. 3(b) and (c)), indicating lower total conductivity in LLZTO/LCBO composites than in LLZTO. Total conductivity at  $27^\circ\text{C}$  is calculated to be  $2.7 \times 10^{-4} \text{ S cm}^{-1}$  for the composite with a LCBO content of 20% and  $2.3 \times 10^{-4} \text{ S cm}^{-1}$  for the composite with a LCBO content of 50%, respectively. It is worth noting that the room temperature conductivity of LLZTO sintered at  $1000^\circ\text{C}$  was in the range of  $10^{-6}\text{--}10^{-5} \text{ S cm}^{-1}$ , indicating that LCBO plays an important role for densification of LLZTO/LCBO composites at low sintering temperature. Due to the larger impedance of LLZTO/LCBO composites than LLZTO, it is slightly difficult to estimate  $R_{\text{int}}$  for LLZTO/LCBO composites, but as confirmed in the impedance data for as-prepared cells, the impedance data below 40–50 kHz may contain the contribution of  $R_{\text{int}}$ . Therefore, we estimated  $R_{\text{int}}$  from the difference in the real part of impedance at 4 Hz and 50 kHz. As results,  $R_{\text{int}}$  for LLZTO/LCBO composites are  $15 \Omega \text{ cm}^2$  and  $20 \Omega \text{ cm}^2$  for LCBO fraction of 20% and 50%, respectively.

Voltage responses in galvanostatic testing at different current densities for symmetric cells with different solid electrolyte pellets are compared in Fig. 4. In each experiment, the initial current density was set to  $0.05 \text{ mA cm}^{-2}$  and increased by  $0.05 \text{ mA cm}^{-2}$  after cycled for 5 cycles. As shown in Fig. 4(a), the symmetric cell with LLZTO are stably cycled at current density up to  $0.30 \text{ mA cm}^{-2}$ , but the sudden drop of cell voltage occurs at  $0.35 \text{ mA cm}^{-2}$  and the voltage response is scattered at current density above  $0.4 \text{ mA cm}^{-2}$ , due to the penetration and propagation of Li dendrite in a solid electrolyte [15, 17–20]. The symmetric cell with LLZTO/LCBO composite with a low LCBO content ( $= 20\%$ ) are stably cycled up to  $0.30 \text{ mA cm}^{-2}$ , while the cell voltage suddenly drops and scatters at  $0.35 \text{ mA cm}^{-2}$  (Fig. 4(b)). However, the abnormal voltage response in the symmetric cell with LLZTO/LCBO composite with a high LCBO content ( $= 50\%$ ) occurs at much lower current density of  $0.15 \text{ mA cm}^{-2}$  (Fig. 4(c)).

As reported in the literatures [4, 15, 17–20], the current densities at which Li dendrite penetrates into a solid electrolyte are strongly influenced from many factors, such as the interfacial connectivity between a Li metal and a solid electrolyte, composition and microstructure of a solid electrolyte such as grain size, porosity and grain boundary structure. Since the difference in  $R_{\text{int}}$  is small between LLZTO and

LLZTO/LCBO composites, the difference in tolerance for Li penetration observed in Fig. 4 is mainly caused by the difference in the compositions and microstructures of LLZTO and LLZTO/LCBO composites. Moreover, Li dendrite penetration in LLZTO/LCBO composite with high LCBO content easily occurs at much lower current density. Although the LCBO addition contributes to the densification of LLZTO at low sintering temperature, excess amount of LCBO additive may result into the degradation of tolerance for Li penetration in solid electrolyte at high current densities.

#### 4. Conclusion

We fabricated garnet-type LLZTO/LCBO composite ceramic solid electrolytes. By adding the appropriate amount of LCBO, composite solid electrolytes were densified by sintering at 1000 °C without covering mother powder and showed room temperature conductivity well above  $1 \times 10^{-4} \text{ S cm}^{-1}$ . Li plating and stripping property for LLZTO/LCBO composites was also evaluated by galvanostatic testing for symmetric cells with Li metal electrodes at room temperature. As results, composite solid electrolyte with LCBO volume content of 20% was stably cycled in a symmetric cell at current density up to  $0.3 \text{ mA cm}^{-2}$ , while the degradation by Li dendrite penetration occurred at much lower current density in composite solid electrolyte with higher LCBO volume content (= 50%). Excess amount of LCBO additive in LLZTO/LCBO composite degraded the tolerance for Li dendrite penetration in a solid electrolyte significantly.

#### Acknowledgements

This work was partly supported by Grant-in-Aid for Scientific Research (JSPS KAKENHI) Grant Number 19H02128 from the Japan Society for the promotion of Science (JSPS). We acknowledged the support of the Cooperative Research Facility Center at Toyohashi University of Technology.

#### References

- [1] F. Zheng, M. Kotobuki, S. Song, M.O, Lei, L. Lu, *J. Power Sources* 389 (2018) 198–213.
- [2] Y. Ren, K. Chen, R. Chen, T. Liu, Y. Zhang, C. Nan, *J. Am. Ceram. Soc.* 98 (2015) 3603–3623.
- [3] R. Murugan, V. Thangadurai, W. Weppner, *Angew. Chem. Int. Ed.* 46 (2007) 7778–7781.
- [4] A.J. Samson, K. Hofstetter, S. Bag, V. Thangadurai, *Energy Environ. Sci.* 12 (2019) 2957–2975.
- [5] K. Tadanaga, R. Takano, T. Ichinose, S. Mori, A. Hayashi, M. Tatsumisago, *Electrochem. Commun.*

- 33 (2013) 51–54.
- [6] N.C. Rosero-Navarro, T. Yamashita, A. Miura, M. Higuchi, K. Tadanaga, *Solid State Ionics* 285 (2016) 6–12.
- [7] S. Ohta, J. Seki, Y. Yagi, Y. Kihira, T. Tani, T. Asaoka, *J. Power Sources* 265 (2014) 40–44.
- [8] L.C. Zhang, J.F. Yang, Y.X. Gao, X.P. Wang, Q.F. Fang, C.H. Chen, *J. Power Sources* 355 (2017) 69–73.
- [9] Y. Ren, T. Liu, Y. Shen, Y. Lin, C. Nan, *J. Materiomics* 2 (2016) 256–264.
- [10] R.D. Shannon, B.E. Taylor, A.D. English, T. Berzins, *Electrochimica Acta* 22 (1977) 783–796.
- [11] T. Okumura, T. Takeuchi, H. Kobayashi, *Solid State Ionics* 288 (2016) 248–252.
- [12] T. Okumura, T. Takeuchi, H. Kobayashi, *J. Ceram. Soc. Jpn.* 125 (2017) 276–280.
- [13] E. Kazyak, K-H. Cheng, A.L. Davis, S. Yu, A.J. Sanchez, J. Lasso, A.R. Bielinski, T. Thompson, J. Sakamoto, D.J. Siegel, N.P. Dasgupta, *J. Mater. Chem. A* 6 (2018) 19425–19437.
- [14] R. Inada, S. Yasuda, M. Tojo, K. Tsuritani, T. Tojo, Y. Sakurai, *Front. Energy Res.* 4 (2016) 28.
- [15] R. Inada, S. Yasuda, H. Hosokawa, M. Saito, T. Tojo, Y. Sakurai, *Batteries* 4 (2018) 26.
- [16] R. Inada, T. Okuno, S. Kito, T. Tojo, Y. Sakurai, *Materials* 11 (2018) 1570.
- [17] C. Tsai, V. Roddatis, C.V. Chandran, Q. Ma, S. Uhlenbruck, M. Bram, P. Heitjans, O. Guillon, *ACS Appl. Mater. Interfaces* 8 (2016) 10617–10626.
- [18] A. Sharafi, E. Kazyak, A.L. Davis, S. Yu, T. Thompson, D.J. Siegel, N. Dasgupta, J. Sakamoto, *Chem. Mater.* 29 (2017) 7961–7968.
- [19] N.J. Taylor, S. Stangeland-Molo, C.G. Haslam, A. Sharafi, T. Thompson, M. Wang, R. Garcia-Mendez, J. Sakamoto, *J. Power Sources* 396 (2018) 314–318.
- [20] X. Huang, Y. Lu, H. Guo, Z. Song, T. Xiu, M.E. Badding, Z. Wen, *ACS Appl. Energy Mater.* 1 (2018) 5355–5365.
- [21] J. Awaka, A. Takashima, K. Kataoka, N. Kijima, Y. Idemoto, J. Akimoto, *Chem. Lett.* 40 (2011) 60–62.

**Figure with captions**

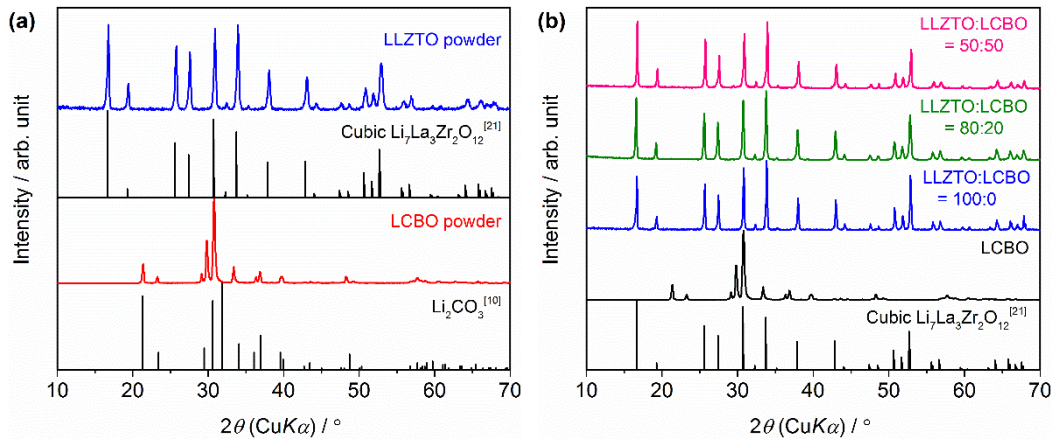


**Fig. 1.** XRD patterns and (a) as-synthesized LLZTO and LCBO powders and (b) LLZTO/LCBO composite pellets. The mixing ratios of LLZTO and LCBO in composites are shown in volume ratios in (b).

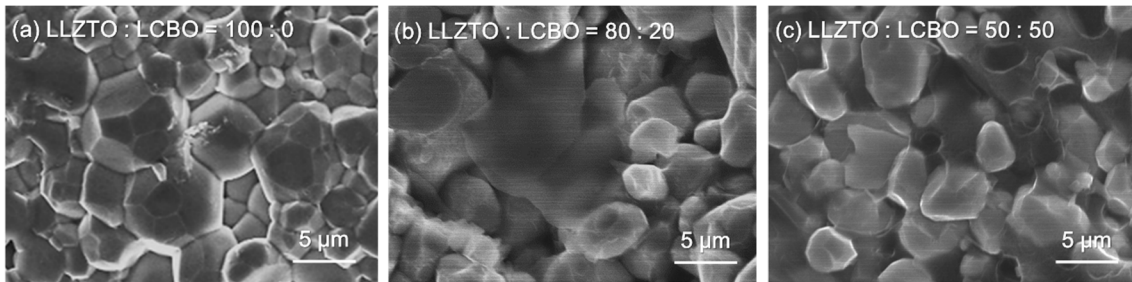


**Fig. 2.** SEM images for fractured cross sections of sintered pellets: (a) LLZTO without LCBO addition, (b) LLZTO/LCBO composite with LCBO content of 20% and (c) LLZTO/LCBO composite with LCBO content of 50%.

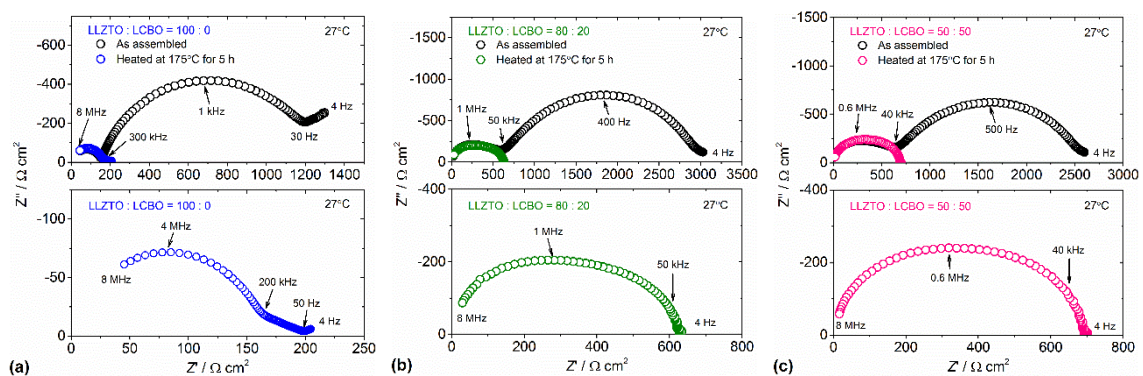


**Fig. 3.** Electrochemical impedance measured at 27°C for symmetric cells before and after heated at 175°C for 5 hours with (a) LLZTO without LCBO addition, (b) LLZTO/LCBO composite with LCBO content of 20% and (c) LLZTO/LCBO content of 50%. Lower graphs show the enlarged plot for each symmetric cell after heated.

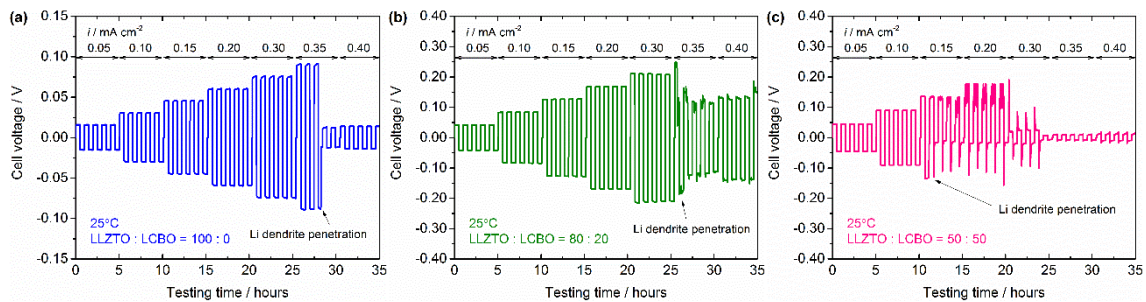


**Fig. 4.** Voltage responses in galvanostatic testing at 25°C for symmetric cells with (a) LLZTO without LCBO addition, (b) LLZTO/LCBO composite with LCBO content of 20% and (c) LLZTO/LCBO composite with LCBO content of 50%.